ADVANCED MATERIALS INTERFACES
Open Access
www.advmatinterfaces.de

Engineering Biofouling Resistant Materials Through the Systematic Adaptation of Surface Morphology

*Emma Sadler, Abish S. Stephen, Robert P. Allaker, and Colin R. Crick**

With increasing numbers of antimicrobial-resistant (AMR) bacteria strains, it becomes essential that new and effective routes to minimizing bacterial infection rates are produced. Superhydrophobic materials show to be effective in reducing the attachment of bacteria due to their unique wetting properties which can minimize the points at which bacteria can initially adhere. Here, the impact of surface design on the anti-biofouling capabilities of superhydrophobic pillared arrays prepared via photolithography is investigated. By systematically varying pillar spacing, insight is gained into the complex nature of superhydrophobic fouling as well as allowing for optimization of the antifouling performance. The optimal material within is achieved at a pillar spacing of 87.5 µm, which shows over a 3-log (and gt; 99.9%) reduction in bacterial attachment.

1. Introduction

The attachment of fouling microbial species to surfaces is a major concern affecting multiple areas of our lives, including healthcare, water distribution systems, marine structures, and food safety. The ubiquitous nature of bacteria and their ability to rapidly colonize a variety of surfaces have proven to be particular issues to our health, leading to increased infection rates and other associated problems such as the failure of orthopedic and dental implants via bacterial-induced infections.[1–5] Over the years, an ever more alarming number of bacteria continue to adapt and become resistant to commonly used antibiotics and disinfectants, with some estimates predicting mortality rates as a result of antimicrobial-resistant (AMR) infections to be as high as 10 million per year globally by 2050 if action is not taken.[2,6,7] After attachment to a surface, bacteria continue to grow and synthesize extracellular polysaccharides, which facilitate adhesion to the surface and other bacteria, thereby increasing the difficulty of removal.[5,8,9] The resulting biofilms, in addition to increased AMR, have made it imperative to develop new effective methods to minimize the spread of bacteria and bacterial infection rates.[10,11] Novel antibacterial materials may help in addressing this by preventing the initial adhesion of bacteria and/or implementing biocidal properties to kill attached bacteria. However, the latter is associated with the risk of accelerating AMR, in addition to toxicity associated with biocidal substances, such as copper or tributyltin.[9,12,13]

Superhydrophobic materials have been shown to reduce the attachment of bacteria with great success with many studies reporting > 90% reduction rates for a variety of strains.[10,14–25] The extremely water-repellent materials are defined by their high water contact angles (>150°) and low tilt angles (<10°).[26,27] The interaction of water with solid surfaces can be explained using either the Wenzel or Cassie–Baxter wetting models. The Wenzel model describes the state in which the surface is fully wetted, having no air within the surface features.[28] For the Cassie–Baxter model, air becomes trapped underneath the water; and so, only the tops of surface features are wetted.[29] As a result of this trapped air, superhydrophobic materials exhibiting Cassie–Baxter wetting behavior allow water droplets to roll across the surface, picking up contamination (including bacteria)—this self-cleaning property is named the "Lotus Effect". This effect is named after the lotus plant, *Nelumbo nucifera,* which is a natural water-repellent plant because of its waxy coating and dual-scale roughness which can trap air beneath water droplets.[30] By designing materials with similar roughened microstructures combined with inherently hydrophobic surface chemistry, superhydrophobic materials capable of reducing bacterial adhesion and the likelihood of biofilm formation can be manufactured.

Despite new functional antibacterial materials being reported each year, limited work has been conducted focusing on the direct impact of surface topology on bacterial adhesion rates. Here, we investigated the impact of pillar spacing on the antibacterial behavior of superhydrophobic micropillar arrays. By modifying the pillar spacing, the roughness, and therefore, the wettability of the material, are altered. When a droplet exists in the Wenzel state, the water contact angle is directly dependent

E. Sadler, C. R. Crick
School of Engineering and Materials Science
Queen Mary University of London
Mile End Road, London E1 4NS, UK
E-mail: c.crick@qmul.ac.uk
A. S. Stephen, R. P. Allaker
Oral Microbiology
Institute of Dentistry
Queen Mary University of London
Newark Street, London E1 2AD, UK

The ORCID identification number(s) for the author(s) of this article can be found under https://doi.org/10.1002/admi.202202532.

DOI: 10.1002/admi.202202532

on the roughness factor, *r*, which is incorporated into the Wenzel model as:[28]

$$\cos\theta_W = r\cos\theta_Y \quad (1)$$

Here, θ_Y is the Young's contact angle for a flat surface and θ_W is the apparent Wenzel contact angle. When a droplet exists in the Cassie–Baxter (CB) state, the water contact angle is now dependent on the solid–liquid fraction, ϕ_S, as shown by the simplified CB equation:[29]

$$\cos\theta_{CB} = \phi_S\cos\theta_Y + \phi_S - 1 \quad (2)$$

From these two equations, we can establish that in the case of full wetting, as pillar spacing increases, the surface roughness decreases, leading to a decreased value of θ_W. When heterogeneous wetting occurs; however, the increased pillar spacing leads to a decreased solid–liquid fraction; and therefore, an increase in θ_{CB}.

Herein, circular pillars in a square array were produced via photolithographic methods and rendered hydrophobic with a thin polydimethylsiloxane (PDMS) coating before exposure to bacterial suspensions of *Staphylococcus aureus* (*S. aureus*), *Escherichia coli* (*E. coli*), or *Streptococcus oralis* (*S. oralis*).

2. Experimental Section

2.1. Materials

Acetone, chloroform, isopropanol, and 1-methoxy-2-propanol acetate (PGMEA) were purchased from Sigma–Aldrich. Glutaraldehyde fixative (EM Grade, 25%), Osmium tetroxide (2% aqueous solution), and UA-Zero EM stain were purchased from Agar Scientific. Paraformaldehyde (4% aqueous solution) and Tannic acid were purchased from Fisher Scientific UK. Photomasks were printed by Micro Lithography Services LTD. P-type silicon wafers (width, 3 in.) were purchased from Pi-Kem. SU8-2050 was purchased from A-gas Electronic Materials. Tryptic soy agar (TSA) and broth (TSB) were purchased from Sigma–Aldrich. *S. aureus* (NCTC 6571), *E. coli* (NCTC 9001), and *S. oralis* (NCTC 11427) were cultured from frozen stocks stored at the Blizard Institute, Queen Mary University of London.

2.2. Fabrication of Superhydrophobic Pillars

2.2.1. Photolithography

Darkfield photomasks were designed in AutoCAD and printed on film to achieve pillars 50 µm in diameter with spacing varying systematically from 37.5 to 250 µm. Before micropatterning, all silicon wafers were cleaned to remove any contamination or dust particles by first rinsing with acetone, followed by isopropanol. After drying the substrate with N_2, SU8-2050 was deposited on the center of the wafer and spun to be evenly distributed at 750 rpm for 15 s and then at 1500 rpm for 30 s. The coated samples were pre-baked at 65 °C, using a heating ramp rate of 1 °C s^{-1} for 10 min, followed by 15 min at 95 °C. UV light was used to define the photomask pattern for 4 s. A post-bake was carried out at 65 °C, using a heating ramp rate of 1 °C s^{-1} for 5 min, followed by 10 min at 95 °C. Samples were then developed using the SU-8 developer PGMEA by submerging and agitating the samples. Isopropanol was then used to clean the samples. If all unlinked SU-8 was not removed, rinsing with PGMEA and isopropanol was repeated until no white residue remained. The final baking step was carried out at 110 °C for 3 min.

2.2.2. PDMS Coating

Sylgard 184 PDMS was prepared by combining the base and curing agent at a 10:1 wt ratio (2.4 g / 0.24 g) and dissolved in chloroform (80 mL). The solution was mechanically stirred for 30 min. The micropatterned silicon wafers (cut into 1 × 1 cm squares) were manually dipped into the coating solution and placed flat to dry on a hotplate set to 80 °C overnight, which also fully cured the thermosetting Sylgard 184.

2.3. Material Characterization

Scanning electron microscopy (SEM) images were obtained using an FEI inspect FESEM operating at an acceleration voltage of 5 kV to minimize charge accumulation and resultant image distortion. To improve the electrical conductivity within the SEM, a thin (≈20 nm) layer of gold was sputter-coated onto the samples. Static water contact angles were recorded using an Ossila Contact Angle Goniometer using 5 µL water droplets. In the Ossila Contact Angle software, baselines were assigned manually. Droplets were placed in five different areas for each sample, with the reported water contact angle (WCA) being the average of these.

2.4. Planktonic Adhesion Assay

Frozen stocks of *S. aureus*, *E. coli*, and *S. oralis* were stored long-term at −80 °C. When required, stocks were defrosted and cultured on TSA in an aerobic atmosphere containing 5% CO_2 at 37 °C. Cultures were maintained by sub-culturing a single colony onto fresh TSA every 3–4 days. A single colony was inoculated into 10 mL TSB followed by incubation overnight at 37 °C. After the incubation period, cultures were pelleted at 3000 g for 10 min, and the pellet resuspended in ≈3 mL of fresh TSB by vortexing. The bacterial suspensions were then diluted in TSB to an OD600 (optical density at 600 nm) value of 0.1. The antibacterial effects of the pillared samples and flat PDMS control were determined using the prepared bacterial suspensions. Samples (1 cm × 1 cm) were submerged and laid flat in 2 mL of bacterial broth suspensions for 1 h in sterile 12-well plates, after which the samples were removed and incubated in 2 mL of fresh TSB in an aerobic atmosphere overnight at 37 °C. After incubation, a sterile swab was run across the entire surface for 5 s and the cells were transferred to 2 mL TSB. Colony-forming units (CFU) were enumerated by serial dilution in TSB with growth of colonies observed on TSA. All tests were performed in triplicate.

ADVANCED MATERIALS INTERFACES
Open Access
www.advmatinterfaces.de

2.5. Fluorescent Microscopy of Attached Bacterial Cells

Fluorescent microscopy samples were initially processed as described in Section 2.4. After overnight incubation, samples were stained using Filmtracer LIVE/DEAD Biofilm Viability Kit (SYTO 9 green-fluorescent nucleic acid stain for live cells, and red-fluorescent nucleic acid stain propidium iodide for dead cells). 200 µL of prepared staining solution was placed onto each sample and left in the dark for 30 min. Samples were then rinsed with filtered sterile DI water and immediately analyzed using an upright Zeiss 710 Laser Scanning Confocal Microscope.

2.6. Scanning Electron Microscopy of Bacterial Cells

SEM of bacterial samples was initially processed as described in Section 2.4. After removal from the broth, samples were fixed overnight with 4% paraformaldehyde and 2.5% glutaraldehyde in 0.1 M phosphate buffer at 4 °C. Samples were fixed again and stained using 2% osmium tetroxide for 1 h, 1% tannic acid for 30 min, and then 2% osmium tetroxide for 1 h.[31] Each stage was followed by thorough rinsing with DI water. Samples were then stained using UA-Zero EM stain overnight at 4 °C. Samples were again rinsed with DI water before successive dehydration with ethanol (30%, 50%, 70%, 80%, and 90% for 15 min and 100% for 30 min). Dehydrated samples were critical-point dried in CO_2 using an EMS K850 Critical Point Dryer (Quorum Technologies). Samples were sputter coated with a thin layer of gold (≈20 nm) and SEM micrographs were then obtained using an FEI inspect F SEM operating at an acceleration voltage of 5 kV.

3. Results and Discussion

3.1. Material Design and Characterization

To investigate the variation in antibacterial functionality with pillar spacing, a series of SU-8 circular pillars was fabricated on silicon wafers. The pillar height (H) and radius (A) were kept constant, while the pillar spacing (*B*) was varied (**Figure 1**). The spacing of the pillars directly impacts both the wetting properties of the resultant materials and the stability of the pillars during production.[32,33] During the photolithography process, errors can occur when producing closely packed high aspect ratio structures as they can easily break or be removed from the substrate during development and drying.[33,34] Capillary forces induce mechanical stress which acts to bend pillars toward each other, creating a deformed pattern or even breaking pillars off the substrate. These errors were minimized by keeping the aspect ratio relatively low (1.6) with A = 50 µm and H = 80 µm. These feature sizes were able to produce highly water repellent surfaces.

SEM was used to image the surfaces and measure the height and diameter of the pillars produced. As evident from the micrographs (Figure 1c), the pillars were successfully formed as designed in the photomask, with damage to surface structures only observable in the areas in which wafers were cut for analysis. By using larger diameter and relatively low aspect ratio pillars, in addition to the use of a low surface tension solvent for washing (isopropanol; surface tension 23 mN m^{-1}), errors (including, the pulling together of pillars and pillar bending) were prevented even as *B* was reduced. SEM showed that the diameter of the micropillars was slightly larger than that of the original photomask (50 µm), averaging 51 ± 1 µm (averaged over 20 readings at various locations). The pillars were observed to have straight sidewalls and lack of T-topping (i.e., no presence of an overhang at the top of the pillars), suggesting no/limited overexposure, and the overall pattern fidelity remained high. Comparison of SEM images before and after PDMS coating allowed the calculation of PDMS film thickness. The film averaged ≈170 nm and was present on the tops and sidewalls of the pillars and the silicon wafer (S4).

The wettability of all samples was examined by measuring WCAs. For samples < 150 µm, care had to be taken when placing droplets on the surface; forcefully placing the droplets

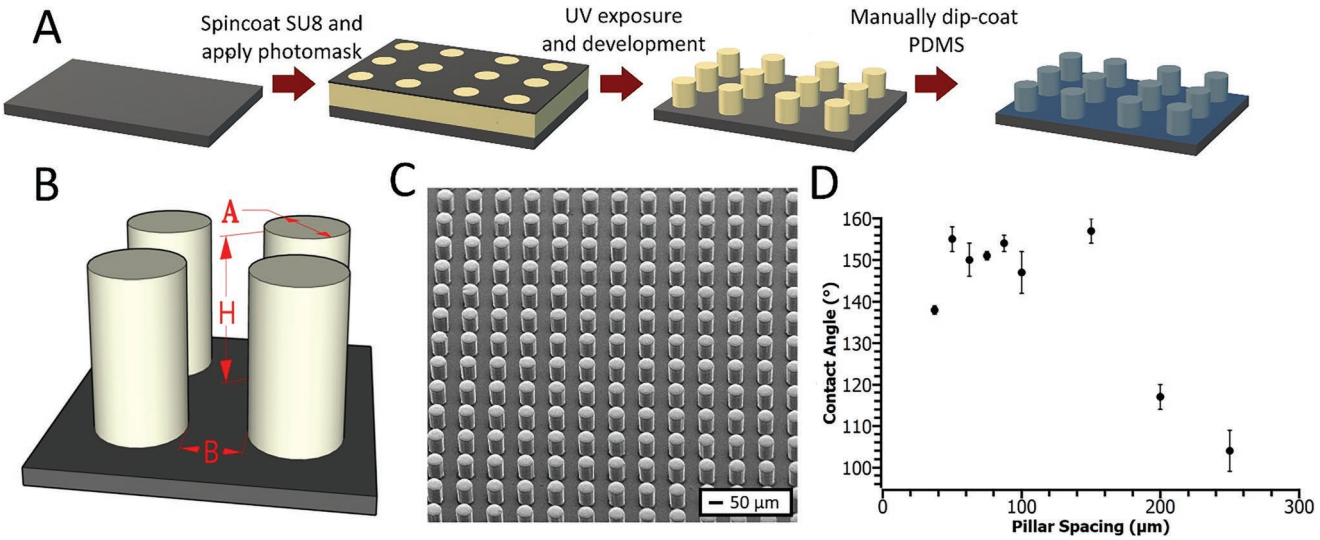

Figure 1. Schematic of A) the fabrication of superhydrophobic pillars on silicon wafers; the negative photoresist (yellow) is spread across the wafer and a photomask (grey) is placed on top before UV exposure and removal of unexposed areas using PGMEA; a thin layer of PDMS (blue) is then applied to increase hydrophobicity. B) Schematic of the circular pillars in a square array where A is the diameter of the pillar, *B* the spacing between, and H height. C) SEM micrographs of pillar array, *B* = 50 µm. D) Plot showing the change in contact angle with pillar spacing.

would result in the water becoming impaled on the surface features, resulting in a lower measured contact angle. PDMS is inherently hydrophobic, measuring a WCA of 99° ± 2° when coated as a flat film on the silicon wafer, and so, when combined with the increased roughness from the micropillar arrays, leads to an amplified hydrophobic effect. The PDMS coated pillars all measured a WCA higher than flat PDMS with the highest value occurring for $B = 150$ µm at 156° ± 3°.

Measured WCAs were consistent with predicted equilibrium CB WCAs (θ_{CB}) up to a pillar spacing of 150 µm, at which point, the WCA begin to steeply drop toward the predicted equilibrium Wenzel angles (see Figure S1, Supporting Information). Although in a CB state (i.e., heterogenous wetting and aligning with theoretical WCAs [Figure S1, Supporting Information]), at a pillar spacing of 37.5 µm, the surface was no longer superhydrophobic with a WCA of 138° ± 1° as a result of the large solid–liquid fraction ($\varnothing_S$) from the densely packed pillars. Though a greater pillar spacing for CB type wetting implies an increased WCA, due to a smaller $\varnothing_S$, the effects of the sagging air–water interface must be considered—particularly at large separations. The denser the pillars are, the more support is given to the water–air interface and a greater extent of sagging depth can be maintained before contact with the substrate. For $B > 200$ µm, the pillar spacing is likely to sparse to accommodate meniscus sagging (see Figure S2, Supporting Information). The result is that the inter-pillar spacing becomes wetted; this reduces air volume and gives WCAs as low as 104° ± 5° ($B = 250$ µm) and sliding angles > 90°. The wetting regime and nature of the resultant wetted interface are key properties for antibacterial functionality as discussed in Section 3.2.

3.2. Bacterial Resistant Properties

The ability of the substrates to resist bacterial attachment was tested using broth cultures of *S. aureus*, *E. coli*, or *S. oralis*. The bacteria selected are all of clinical significance covering both Gram-positive/negative as well as motile and non-motile species.[35,36] *S. aureus* and *E. coli* are some of the top bacterial pathogens contributing to global deaths associated with AMR with both being listed by the World Health Organization (WHO) in 2017 as part of the twelve "priority pathogens" posing the greatest threats to human health.[7,31,37] Streptococci are a Gram-positive species that have been found to have a substantial impact on biofilm formation within the human oral cavity, the growth of which can greatly impact the success of dental implants.[38,39]

Flat PDMS wafers (hydrophobic) were also included as control samples. The reduction in viable cells adhering to the surface was then examined by extracting cells with sterile swabs. To enumerate the viable cells, serial dilutions were carried out in TSB; the diluted bacterial broth was then plated onto TSA. After incubation, the number of colonies could be counted and the CFU per mL was calculated (**Figure 2**).

$$\text{CFU} = \frac{\text{No. of colonies} \times \text{dilution factor}}{\text{Vol. of cultured plate}} \tag{3}$$

A full presentation of the CFU reduction data is provided in **Figure 3**. In this, a reduction in viable *S. aureus* CFU compared to flat PDMS was observed for six of the nine samples (Figure 3A). Pillar spacings between 50 and 150 µm showed

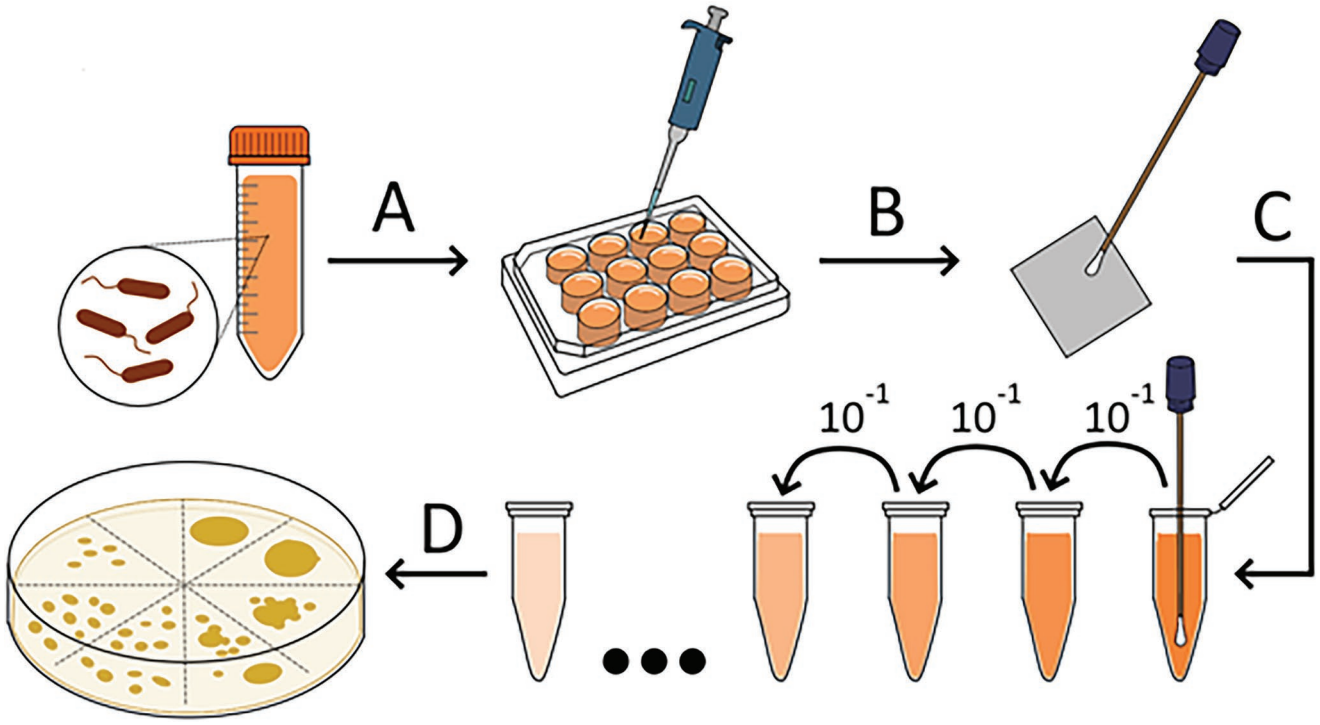

Figure 2. Schematic of experimental method for planktonic adhesion assay. A) Cultures of bacteria were prepared and adjusted to an initial OD600 value of 0.1. Samples were placed in a 12-well plate with cultured broth and incubated overnight. B) After removal form broth, the surfaces were swabbed to collect adhered bacteria. C) After overnight, incubation samples were swabbed to collect adhered bacteria, serially diluted, and serially diluted, and then D) plated for CFU counts.

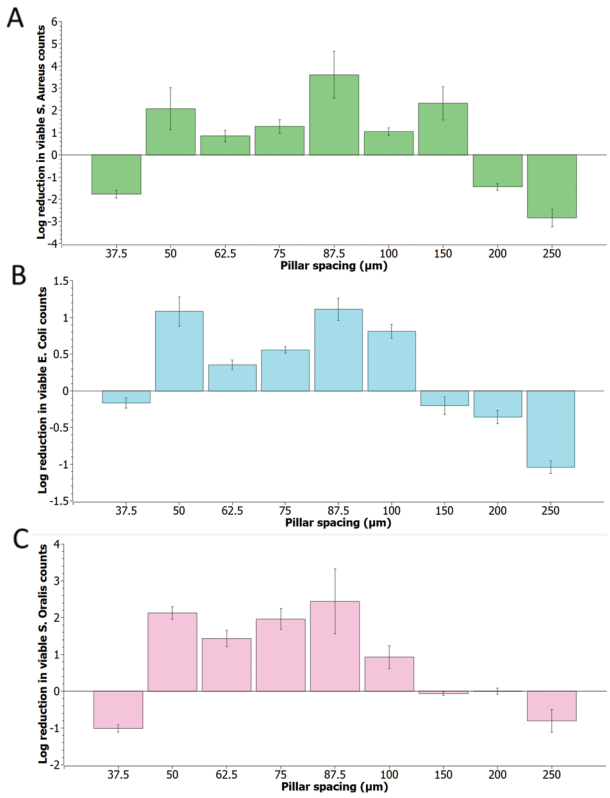

Figure 3. Data for the log reduction in viable bacterial cells extracted from the surface compared to flat PDMS for A) *S. aureus*, B) *E. coli*, and C) *S. oralis* using PDMS coated pillars with various separation distances.

a reduction in viable cell counts of 85–99.9%, with the largest reduction being observed at B = 87.5 μm, which displayed a 99.9% reduction (a 3.6 log reduction) compared to flat PDMS. The pillar spacings used during the study (37.5–250 μm) were significantly larger than the average bacterium size (0.2–2.0 μm), meaning that failure of the liquid–air interface may expose the bacteria to an increased area for attachment. For samples with pillar spacing > 150 μm, the WCAs discussed in Section 3.1 indicate that Wenzel type wetting is occurring. The surface features are fully wetted, and as a result, have an increased surface area over which bacteria can initially attach, leading to increased viable cell counts A similar result is observed for *E. coli* (Figure 3B) and *S. oralis* (Figure 3C) samples, for which five of the nine samples showed a reduction in colony forming units. For these cultures, samples with pillar spacing between 50 and 100 μm showed a reduction between 55% and 92% and between 88% and 99% for *E. coli* and *S. oralis*, respectively. Though B = 150 μm had the highest static contact angle measurement and showed a 99% reduction (a 2.3 log reduction) in viable *S. aureus* counts compared to flat PDMS, for these bacteria, an increase in attachment was now observed. The bacteria in the solution would modify the surface tension of the liquid which could account for B = 150 μm no longer showing antibacterial effects for both *E. coli* and *S. oralis*.[40]

As expected, when comparing samples with Wenzel type wetting to those with CB type wetting, an increased number of bacteria are seen to have attached to the surface, as a result of the increased water–solid contact. When considering CB type wetting, several additional factors further influence the overall effectiveness of a material's bacterial resistant functionality. First, the solid–liquid fraction ($\varnothing_S$): as bacteria in the chosen assays are present in the aqueous phase and no biocides are present, all reductions can be primarily attributed to the minimization of points to which bacteria can attach and grow. $\varnothing_S$ has a direct correlation with bacterial adhesion, such that, when $\varnothing_S$ decreases by increasing the pillar spacing, the area available for bacteria to adhere to is reduced. This area is instead replaced by a greater liquid–vapor phase, which is not viable for bacterial adhesion. In addition to fewer adhesion points, the greater volumes of trapped air limit diffusion, the process by which nutrients and solute are transported to/from cells within a biofilm.[41] The air layer is a low nutrients environment; and therefore, reduces the biofilms ability to spread and colonize further on the surface. Both *S. aureus* and *S. oralis* are non-motile bacteria and tend to sediment readily. This means for the hydrophobic PDMS, which has complete solid–liquid contact, as the bacteria settles, it becomes positioned on the surface ready for attachment. When we introduce superhydrophobicity, this settlement of bacteria in combination with the slight curvature of pillar tops (Figure S3, Supporting Information) causes the bacteria to collect in the bridging water, away from the adhesion points of the pillars. As we increase the pillar spacing to reduce $\varnothing_S$, we additionally change the degree to which the water sags between the pillars (Figure S2, Supporting Information). As the curvature increases, the bacteria will be held further away, reducing the overall adhesion; however, if the curvature of the bridging water becomes too great, this will then touch the substrate bottom between the pillars, allowing the bacteria to be exposed to a larger area for adhesion once again. *E. coli*, unlike the other two bacteria being investigated, is a motile strain and as such, can actively search for the surface to adhere to, meaning the influence of sagging water is less effective in limiting the attachment of these bacteria. The motility of the bacteria clearly impacts biofilm formation in the horizontal set-up used for the assays and could explain why the reductions in viable cell counts is much lower for the *E. Coli* strain (Figure 3). The horizontal position was chosen as it allows for a straightforward experimental set-up which provided a great degree of experimental reproducibility. In addition, the stability and morphology of the trapped air layer would also be maintained. It is expected that an alternative substrate orientation (e.g., vertical) has the potential to provide a different measure of biofilm prevention (due to the lessened effect of settling non-motile bacteria). However, this has the potential to introduce other experimental variables but should perhaps form part of a future study. Last, we should also be aware of the dynamic effects that are occurring as the samples are removed from the liquid broth. Superhydrophobic materials allow water to roll across the surface and remove bacteria as it does. Before doing so, droplets are "pinned" to the surface features. Depinning must occur before the droplet can roll with the force required to do so varying between samples, with this being greatest for materials showing Wenzel type wetting.[42] As pillars become more spaced out, the number of pinning points is reduced, contributing to a lower amount of pinning force and easier

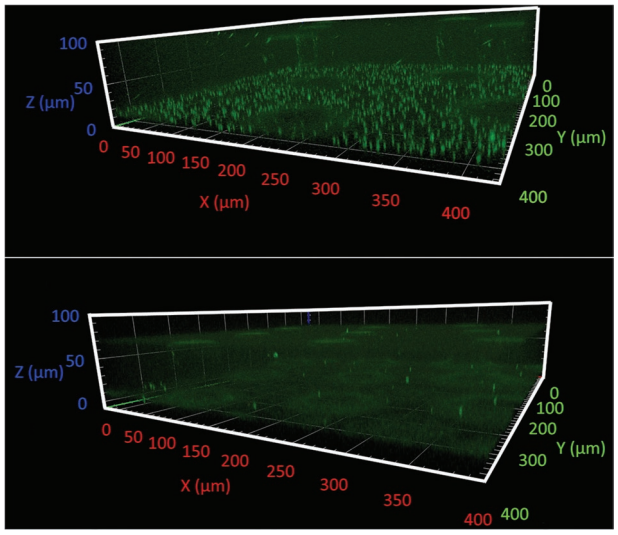

Figure 4. Confocal laser scanning microscope images of live (bright green) *E. coli* on PDMS-coated pillars where (top) B = 150 μm and (bottom) B = 100 μm.

removal of all liquid (and bacteria); however, this occurs at the risk of an increased number of micro-droplets being left stuck to pillars as a result of pillars penetrating the rolling droplets. Removal of water aids in carrying non-strongly adhered bacteria away, whilst stuck microdroplets leave bacteria close to the surface where they can again adhere.[43] All these factors must be considered and balanced when designing optimal surfaces for bacterial attachment resistance; within our testing range, a pillar spacing of 87.5 μm gave the greatest trade-off between factors to achieve over 3-log reductions (reduction up to 99.9%).

The swabbing techniques used for the CFU measurements (Figure 3) probe the overall presence of bacteria. In order to identify the precise location of bacterial attachment, 3D fluorescence confocal microscopy images were taken (**Figure 4**; Figure S5, Supporting Information). For samples with B = 150 μm (which showed a 37.5% increase in attached *E. coli*), most of the bacteria were observed at the bottom of surface features with some bacteria present on the sides and tops of pillars as well. As previously mentioned, the bacteria in the solution affect the wettability and this image confirms that through recording a static WCA of 156° ± 3° within the bacterial solution, the surface was unable to maintain the layer of trapped air, resulting in complete wetting of the surface and exposing the bacteria to a larger area over which to attach. In contrast, the B = 100 μm sample, in addition to showing minimal live bacteria (bright green), showed only attachment on the tops and sides of the pillars. Here, the air layer was maintained during the testing period and the reduced liquid–solid contact minimized bacterial adhesion points to achieve an 84% reduction in attached *E. coli*. The live–dead study showed no dead bacteria (red), further highlighting that the antibacterial effect is purely a result of repulsion caused by surface chemistry/morphology.

Further SEM analysis was undertaken to observe the attachment of cells and the presence of extracellular matrix. These images (**Figure 5**) show that most of the bacterial attachment is occurring on the top of pillars with minimal bacteria

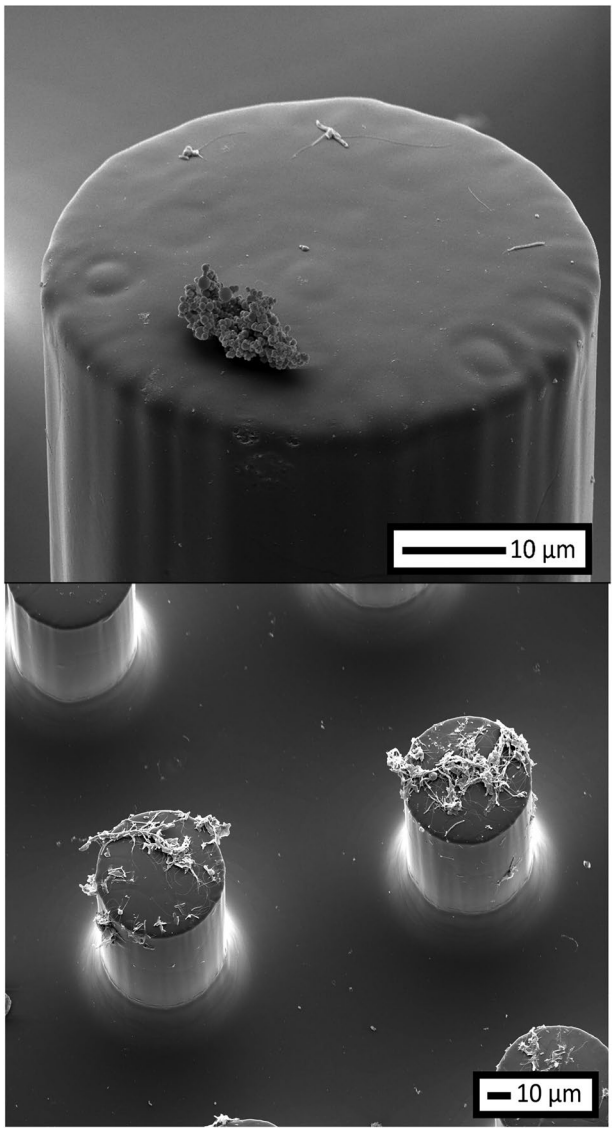

Figure 5. SEM micrographs of *S. aureus* showing the attachment of bacteria on PDMS-coated pillar tops (B = 75 μm) and the beginning of biofilm formation.

present on the bottom of samples showing large reductions >90% (agreeing with fluorescence imaging results). The images also reveal that the bacteria on the top of pillars are primarily adhering through cell–cell interactions to other bacteria, with only a minimal number attached directly to the surface as the bacteria grow away from the surface features. Despite the relatively small culture period, the production of extracellular matrices can already be observed, which is limited to the top of the pillars.

4. Conclusion

Though much work has been done on the antibacterial properties of superhydrophobic materials in addition to the impact of surface features on wettability, very little has focused on

the direct effect of surface features on the overall antibacterial functionality.[16,22–25,31,32,44,45] Here, we begin that discussion by investigating the effects of surface topology, specifically the spacing of pillars, on the antibacterial properties of PDMS-coated pillars. By varying the spaces between pillars using targeted photolithographic methods, an array of samples was produced that possessed a range of wettabilities; from flat PDMS with a contact angle of 99° ± 2° up to 156° ± 3° at a pillar spacing of 150 µm. The relative success of the materials within this array is shown to be a combination of multiple factors in a complex relationship which determine the effectiveness of repelling bacteria. The four main components that contribute to the antibacterial properties are namely, wetting type (CB vs Wenzel), liquid–air interface curvature, solid–liquid fraction, and water pinning forces. Within our sample size, a pillar spacing of 87.5 µm showed the highest bacterial repulsion results appearing as the optimal trade-off of factors, allowing for reductions in bacterial attachment (up to >99.9%). The work within focuses on planktonic bacterial adhesion; future work should now consider biofilm formation and other surface features (aspect ratio, pillar shape etc.). Furthermore, an effective antibacterial material should further be active across multiple bacterial strains, and as such, a logical next step is to expand the bacterial assay. Systematic studies, such as the reported work, are a key step in developing bacteria-resistant surfaces for the real world as they will identify morphologies and chemistries best suited to these applications.

Supporting Information

Supporting Information is available from the Wiley Online Library or from the author.

Acknowledgements

C.R.C. would like to thank the EPSRC for research funding. E.S. would like to thank Liisa Blowes and the Cross-InstitutE Tissue Engineering (CREATE) lab for their assistance with photolithography.

Conflict of Interest

The authors declare no conflict of interest.

Data Availability Statement

The data that support the findings of this study are available from the corresponding author upon reasonable request.

Keywords

anti-fouling, biofouling, photolithography, superhydrophobic surfaces

Received: January 3, 2023
Revised: February 8, 2023
Published online:

[1] B. Li, T. J. Webster, *J. Orthop. Res.* **2018**, *36*, 22.
[2] I. C. Stanton, A. Bethel, A. F. C. Leonard, W. H. Gaze, R. Garside, *Environ. Evidence* **2022**, *11*, 8.
[3] J. S. Dhaliwal, N. A. Abd Rahman, L. C. Ming, S. K. S. Dhaliwal, J. Knights, R. F. Albuquerque Junior, *Front. Cell. Infect. Microbiol.* **2021**, *11*, 1.
[4] U. Mahanta, M. Khandelwal, A. S. Deshpande, *J. Mater. Sci.* **2021**, *56*, 17915.
[5] S. Kreve, A. C. D. Reis, *Jpn. Dent. Sci. Rev.* **2021**, *57*, 85.
[6] P. Shankar, *Arch. Pharm. Pract.* **2016**, *7*, 110.
[7] C. J. Murray, K. S. Ikuta, F. Sharara, L. Swetschinski, G. Robles Aguilar, A. Gray, C. Han, C. Bisignano, P. Rao, E. Wool, S. C. Johnson, A. J. Browne, M. G. Chipeta, F. Fell, S. Hackett, G. Haines-Woodhouse, B. H. Kashef Hamadani, E. A. P. Kumaran, B. McManigal, R. Agarwal, S. Akech, S. Albertson, J. Amuasi, J. Andrews, A. Aravkin, E. Ashley, F. Bailey, S. Baker, B. Basnyat, A. Bekker, et al., *Lancet* **2022**, *399*, 629.
[8] Y. A. Mehanna, E. Sadler, R. L. Upton, A. G. Kempchinsky, Y. Lu, C. R. Crick, *Chem. Soc. Rev.* **2021**, *50*, 6569.
[9] G. Gebreyohannes, A. Nyerere, C. Bii, D. B. Sbhatu, *Heliyon* **2019**, *5*, e02192.
[10] X. Yang, W. Zhang, X. Qin, M. Cui, Y. Guo, T. Wang, K. Wang, Z. Shi, C. Zhang, W. Li, Z. Wang, *Biomimetics* **2022**, *7*, 88.
[11] L. Wang, X. Guo, H. Zhang, Y. Liu, Y. Wang, K. Liu, H. Liang, W. Ming, *Coatings* **2022**, *12*, 1469.
[12] G. Gizer, U. Önal, M. Ram, N. Sahiner, *Biointerface Res. Appl. Chem.* **2023**, *13*, 1.
[13] L. P. Arendsen, R. Thakar, A. H. Sultan, *Clin. Microbiol. Rev.* **2019**, *32*, e00125.
[14] R. L. Upton, R. A. Dop, E. Sadler, A. M. Lunt, D. R. Neill, T. Hasell, C. R. Crick, *J. Mater. Chem. B* **2022**, *10*, 4153.
[15] E. Ozkan, C. C. Crick, A. Taylor, E. Allan, I. P. Parkin, *Chem. Sci.* **2016**, *7*, 5126.
[16] C. R. Crick, S. Ismail, J. Pratten, I. P. Parkin, *Thin Solid Films* **2011**, *519*, 3722.
[17] J. Seyfi, M. Panahi-Sarmad, A. OraeiGhodousi, V. Goodarzi, H. A. Khonakdar, A. Asefnejad, S. Shojaei, *Colloids Surf., B* **2019**, *183*, 110438.
[18] H. Agbe, D. K. Sarkar, X. G. Chen, *Coatings* **2020**, *10*, 982.
[19] Y. Lin, H. Zhang, Y. Zou, K. Lu, L. Li, Y. Wu, J. Cheng, Y. Zhang, H. Chen, Q. Yu, *J. Mater. Sci. Technol.* **2023**, *132*, 18.
[20] W. Li, K. Liu, Y. Zhang, S. Guo, Z. Li, S. Ching, *Chem. Eng. J.* **2022**, *446*, 137195.
[21] Y. Zhan, S. Yu, A. Amirfazli, A. Rahim Siddiqui, W. Li, *Adv. Eng. Mater.* **2022**, *24*, 2101053.
[22] V. K. Manivasagam, G. Perumal, H. S. Arora, K. C. Popat, *J. Biomed. Mater. Res., Part A* **2022**, *110*, 1314.
[23] M. Ayazi, N. Golshan Ebrahimi, E. J. Nodoushan, *Int. J. Adhes. Adhes.* **2019**, *88*, 66.
[24] F. Sahin, N. Celik, A. Ceylan, S. Pekdemir, M. Ruzi, M. S. Onses, *Chem. Eng. J.* **2022**, *431*, 133445.
[25] J. Seyfi, V. Goodarzi, F. R. Wurm, S. Shojaei, M. Jafari-Nodoushan, N. Najmoddin, H. A. Khonakdar, M. H. Baghersad, L. Uzun, *Prog. Org. Coat.* **2020**, *149*, 105944.
[26] E. Sadler, C. R. Crick, *Sustainable Mater. Technol.* **2021**, *29*, e00321.
[27] R. L. Upton, Z. Davies-Manifold, M. Marcello, K. Arnold, C. R. Crick, *Mol. Syst. Des. Eng.* **2020**, *5*, 477.
[28] R. N. Wenzel, *Ind. Eng. Chem.* **1936**, *28*, 988.
[29] A. B. D. Cassie, S. Baxter, *Trans. Faraday Soc.* **1944**, *40*, 546.
[30] W. Barthlott, C. Neinhuis, *Planta* **1997**, *202*, 1.
[31] A. Susarrey-Arce, I. Sorzabal-Bellido, A. Oknianska, F. McBride, A. J. Beckett, J. G. E. Gardeniers, R. Raval, R. M. Tiggelaar, Y. A. Diaz Fernandez, *J. Mater. Chem. B* **2016**, *4*, 3104.
[32] K. Smyth, A. Paxon, H. M. Kwon, T. Deng, K. K. Varanasi, in *2010 12th IEEE Intersociety Conf. Thermal and Thermomechanical Phenomena in Electronic Systems*, IEEE, Piscataway, NJ **2010**, pp. 1–8.

[33] L. Amato, S. S. Keller, A. Heiskanen, M. Dimaki, J. Emnéus, A. Boisen, M. Tenje, *Microelectron. Eng.* **2012**, *98*, 483.
[34] H. J. Lee, J. T. Park, J. Y. Yoo, I. An, H. K. Oh, *J. Korean Phys. Soc.* **2003**, *42*, 202.
[35] L. G. Harris, S. J. Foster, R. G. Richards, P. Lambert, D. Stickler, A. Eley, *Eur. Cells Mater.* **2002**, *4*, 39.
[36] J. B. Kaper, J. P. Nataro, H. L. T. Mobley, *Nat. Rev. Microbiol.* **2004**, *2*, 123.
[37] World Health Organisatoin, "2019 ANTIBACTERIAL AGENTS IN CLINICAL DEVELOPMENT: an analysis of the antibacterial clinical development pipeline," https://apps.who.int/iris/bitstream/handle/10665/330420/9789240000193-eng.pdf, **2019**.
[38] R. Liu, K. Memarzadeh, B. Chang, Y. Zhang, Z. Ma, R. P. Allaker, L. Ren, K. Yang, *Sci. Rep.* **2016**, *6*, 29985.
[39] S. Dhir, *J. Indian Soc. Periodontol.* **2013**, *17*, 5.
[40] Y. Zhao, B. Jeong, D. H. Kang, S. Dai, in *E3S Web of Conf* **2020**, *205*, https://doi.org/10.1051/e3sconf/202020508003.
[41] P. S. Stewart, *J. Bacteriol.* **2003**, *185*, 1485.
[42] Y. Jiang, *Surf. Innov.* **2022**, *10*, 373.
[43] W. S. Y. Wong, T. P. Corrales, A. Naga, P. Baumli, A. Kaltbeitzel, M. Kappl, P. Papadopoulos, D. Vollmer, H. J. Butt, *ACS Nano* **2020**, *14*, 3836.
[44] R. L. Upton, C. R. Crick, *Mol. Syst. Des. Eng.* **2020**, *5*, 477.
[45] Z. Montgomerie, K. C. Popat, *Mater. Sci. Eng., C* **2021**, *119*, 111503.